

## Three-dimensional effects in turbulent bluff-body wakes

By ANIL PRASAD AND CHARLES H. K. WILLIAMSON

Mechanical and Aerospace Engineering, Cornell University, Ithaca, NY 14853, USA

(Received 2 December 1996 and in revised form 14 February 1997)

There has recently been a surge in activity concerning the development of three-dimensionality in the wakes of nominally two-dimensional bluff bodies, yielding the realization that end effects can influence the wake vortex shedding pattern over long spanlengths. Much of this work has been focused on low Reynolds numbers ( $Re$ ), but virtually no studies have investigated to what extent it is possible to control shedding patterns at higher Reynolds numbers, through the use of end manipulation. In the present paper, we demonstrate that it is possible to induce parallel shedding, oblique shedding and vortex dislocations, by manipulation of the end conditions, over a large range of Reynolds number. Such patterns affect the frequency of primary wake instability and its amplitude of fluctuation, as they do at low Reynolds number, although distinct differences are found at the higher Reynolds numbers.

We find that imposition of oblique shedding conditions at high Reynolds number leads to a spatial variation of both the oblique shedding angle and shedding frequency across the span, and to sparse dislocations which are not restricted to the spanwise end regions, as they are at low Reynolds numbers (under similar geometrical conditions). In the wake transition regime ( $Re = 190\text{--}250$ ), it is confirmed that the spontaneous appearance of vortex dislocations in mode-A shedding precludes the control of shedding patterns using end manipulation. However, it has proven possible to extend the regime of Reynolds number where dislocations ‘naturally’ exist to  $Re > 250$ , by introducing them artificially through end control, where they would otherwise not occur. The possibility of introducing dislocations and of inducing oblique vortex shedding at higher Reynolds numbers has practical significance, if one can deliberately decorrelate the vortex shedding, and hence reduce the spanwise-integrated unsteady fluid forces on the body.

We confirm the existence of a transition in the mode of shedding at  $Re \approx 5000$  (originally found by Norberg 1987) under conditions where parallel shedding is attempted. This mode transition displays similarities to an inverse of the mode A  $\rightarrow$  mode B transition that is found in the wake transition regime. It is clear that vortex dislocations occur beyond  $Re = 5000$ , although it is not clear why the flow is unstable to such a mode. Furthermore, there appears to be some support for the suggestion that vortex dislocations may be a feature of the flow for  $Re$  at least up to  $30 \times 10^3$ , as evidenced by the work of Norberg (1994).

---

### 1. Introduction

The study of bluff-body flows has been a subject of interest to engineers and scientists for several decades. The abundance of phenomena observed in bluff-body

flows is a direct consequence of the fact that these flows are actually composed of three fundamental shear flows, namely the wake, the separated shear layer and the boundary layer, each of which develops instabilities as the Reynolds number ( $Re$ ) is progressively increased. The focus of the present investigation is the wake behind a circular cylinder.

It is known that the fundamental wake instability results in the formation of the classical von Kármán street configuration for  $Re > 49$ . The two-dimensional aspects of this wake instability are well-understood, and have been explained in the context of a Hopf bifurcation (Provansal, Mathis & Boyer 1987). However, it is only recently that a large number of investigations have been concerned with the development of three-dimensional structure in cylinder wakes. Many of these recent developments have been reviewed comprehensively by Williamson (1996a). It is perhaps not surprising that the bulk of the recent experimental efforts has focused on low Reynolds numbers, where smaller scales have not yet developed. A number of new flow phenomena have been discovered, many of which are influenced by the spanwise end boundary conditions on the cylinder. However, virtually no studies have been undertaken to investigate the presence of these new phenomena at moderate and high Reynolds numbers, and to study the possible control of three-dimensional wake patterns by manipulating the end boundary conditions. The possibility of control on the shedding pattern has corresponding implications for the control of unsteady fluid forces experienced by the body. This practical question provides the main motivation for the present study.

In the case of low Reynolds numbers, several three-dimensional phenomena have been observed. In the following discussion, we use the definitions and nomenclature of Williamson (1996a) for various vortex shedding regimes. In the laminar shedding regime ( $49 < Re < 190$ ), characterized by periodic wake velocity fluctuations, it has been found that one can induce both oblique shedding and parallel shedding over long spans, by manipulating the end conditions. The phenomenon of oblique shedding provides an explanation for the observation of discontinuities in the variation of the Strouhal number ( $S = f_K D / U_\infty$ , where  $f_K$  is the vortex shedding frequency) with Reynolds number. By manipulating the end conditions to produce parallel vortex shedding, Williamson (1988a, 1989) found that a completely continuous Strouhal–Reynolds number variation can be realized. Although he used angled endplates to promote parallel shedding over long spanlengths, several other techniques have also been successfully used to achieve the same effect, including ending the cylinder with larger coaxial cylinders (Eisenlohr & Eckelmann 1989), locating larger cylinders normal to and upstream of the test cylinder (Hammache & Gharib 1991), and using a non-mechanical end-suction technique (Miller & Williamson 1994; Monkewitz, Williamson & Miller 1996). It appears that each of these techniques involves a slight local increase of velocity near the ends and an increase of the local base suction giving an end condition which induces parallel shedding across the entire span. In addition to determining a continuous  $S$ – $Re$  relationship for parallel shedding, Williamson (1988a, 1989) also found that the oblique shedding data ( $S_\theta$ ) could be collapsed onto the parallel shedding data ( $S_0$ ) by a cosine transformation,

$$S_\theta = S_0 \cos \theta, \quad (1.1)$$

where  $\theta$  is the vortex shedding angle. This cosine transformation has subsequently been confirmed by several other investigators, in the laminar shedding regime, for vortex shedding angles ranging from  $0^\circ$  to  $20^\circ$ .

Although it has been known for several years that it is possible to control oblique and parallel modes of vortex shedding at low Reynolds numbers, it appears surprising

that such control, over long spanlengths, has not been attempted at higher Reynolds numbers. One naturally questions whether the end boundary conditions which control the vortex shedding pattern in the laminar shedding regime, continue to do so for  $Re > 190$ . It is with this question that we commence the present study. The motivation for such a study lies in its importance to the spanwise-integrated unsteady fluid forces on a body; these forces which arise from the vortex shedding process, depend on the phase of shedding and its correlation along the span. Clearly, when oblique shedding is induced, the unsteady fluid forces on the body are not in phase along the span as a consequence of the spanwise variation of the shedding phase, thereby producing a small spanwise-integrated unsteady fluid force on the body. However, by inducing parallel shedding and a constant shedding phase, much larger spanwise-integrated unsteady fluid forces would be measured.

In addition to the oblique shedding modes found in the laminar shedding regime, one also observes the phenomenon of cellular shedding, whereby cells of different frequencies coexist at different spanwise locations. Although Gerich & Eckelmann (1982) found that a cell of lower frequency appears near the end of the cylinder, due to the direct influence of the end boundary condition, Williamson (1988*a*, 1989) and König, Eisenlohr & Eckelmann (1990) showed that a cell of lower frequency can occur in the central portion of the span of a cylinder which is even hundreds of diameters long. In the region between these spanwise cells are found large-scale three-dimensional structures called 'vortex dislocations' (Williamson 1989), also referred to as 'vortex splitting' (Eisenlohr & Eckelmann 1989). These dislocations, whereby vortices move in and out of phase with neighbouring vortices, are found to be a fundamental aspect of the transition to three-dimensionality in the cylinder wake.

The transition to three-dimensionality which occurs over the range  $190 < Re < 260$ , involves two discontinuous changes in the Strouhal–Reynolds number relationship (Williamson 1988*b*, 1996*b*). At the first discontinuity, which is hysteretic, the Strouhal frequency drops from the laminar shedding curve to the mode-A three-dimensional shedding curve, at  $Re = 180$ – $190$ . As  $Re$  is increased up to  $230$ – $260$ , another discontinuity manifests itself and the Strouhal number rises to the mode-B three-dimensional shedding curve. This latter discontinuity is, however, not hysteretic, but instead involves the gradual transfer of energy from mode A to mode B, as  $Re$  is increased. At the first discontinuity, the peak at the shedding frequency (in long-time-averaged velocity spectra) exhibits two possible shapes at the same  $Re$ , due to the hysteresis effect. However, at the second discontinuity, the spectra are 'twin-peaked', due to an intermittent swapping from mode A to mode B, rather than the simultaneous existence of both modes (Williamson 1996*b*). These two modes in the transition regime are distinguished by their distinct spanwise structures. In mode-A shedding, the primary vortices deform in a wavy fashion along their span during the shedding process, due to the action of an elliptic vortex-core instability (Williamson 1996*b*; Leweke & Williamson 1996). This results in the formation of vortex loops, which subsequently become stretched into streamwise vortex pairs. At higher  $Re$ , when mode-B shedding manifests itself, finer-scale streamwise vortex pairs are formed.

The existence of the mode-A and mode-B small-scale structures in the wake transition regime is complemented by the presence of the much larger three-dimensional structures referred to earlier, called vortex dislocations. In an extensive study, Williamson (1992) showed that the large low-frequency irregularities observed in wake velocity fluctuations measured in the transition regime are due to the existence of vortex dislocations. These dislocations which grow to immense proportions in streamwise and spanwise extent (of the order of 100 diameters) are responsible for

the slow downstream decay of wake velocity fluctuations. Williamson (1996*b*) also demonstrated that in the transition regime, two-sided vortex dislocations are found to be generated spontaneously along the span, and that they differ from the one-sided dislocations found near the ends of the cylinder. An important question which we address in the present paper is whether vortex dislocations are present in the cylinder wake for Reynolds numbers above the transition regime, and indeed if they can be artificially induced where they would not otherwise occur.

In the light of a new understanding of phenomena discovered at low Reynolds numbers, it has been found that the end boundary conditions on the cylinder can control many spanwise three-dimensional structures. However, there has been apparently no study which shows to what extent these low-Reynolds-number phenomena occur at higher Reynolds numbers. Although the work of Stäger & Eckelmann (1991) demonstrated that an end cell of lower frequency forms near the end condition even at  $Re$  above the laminar shedding regime, there has been virtually no work to investigate the control of three-dimensional phenomena over long cylinder spans of the order of 50 diameters. This paper, in which we investigate the possibility of such end boundary condition control, has been organized in the following manner. Following a brief description of the experimental details in §2, in §3 we begin by providing evidence for the control of the shedding pattern at moderately high Reynolds numbers. We will show that parallel and oblique shedding can be induced by simply manipulating the end conditions, although in the latter case there appears to be some spanwise variation in the mean shedding angle. We then characterize measured parameters in the wake for parallel and oblique shedding end conditions, in §4, over a large range of Reynolds number. These measurements provide a basis for us to examine in detail various aspects of the effect of end boundary condition control on the wake pattern over particular ranges of  $Re$ . In §5, we focus specifically on the wake transition regime, and show that the spontaneous generation of vortex dislocations precludes control of the shedding pattern; however, we will show that control is regained at the upper end of the transition regime. This is followed in §6 by an investigation of the influence of cylinder aspect ratio which indicates that, for long spanlengths, there may be some spanwise variation of the shedding angle when oblique shedding end conditions are imposed. Based on some preliminary observations made in §4 regarding the transition at  $Re = 5000$ , we return with detailed measurements in §7 and confirm the existence of this transition which was previously observed by Norberg (1987). Furthermore, we suggest from these measurements that a mode change occurs at this Reynolds number due to the inception of vortex dislocations. Following this, we present some concluding remarks.

## 2. Experimental details

The experiments were performed in an open-circuit suction wind tunnel. The free-stream turbulence was less than 0.08% and flow uniformity better than 0.3% in the 12 in.  $\times$  12 in. test section. Cylinders of diameter 0.108, 0.318 and 0.635 cm were mounted near the upstream end of the test section. The Reynolds number is defined as  $Re = U_\infty D/\nu$ , where  $U_\infty$  is the free-stream velocity and  $D$  is the cylinder diameter. Endplates (of diameter =  $20D$ ) fitted on the cylinder produced aspect ratios ( $L/D$ ) of 40–200, where  $L$  is the distance between the endplates. Our flow visualizations indicate that the endplates directly influence about 8–10 diameters of the cylinder span. However, despite the presence of these end regions, a significant portion (around 80%) of the span remains unaffected, for the cylinder of aspect ratio 80. However,

for smaller ratios, one expects the unaffected region, based on the measurements of Stäger & Eckelmann (1991) and Miller & Williamson (1994), to be of the order of 50%–55%.

The origin of the wake coordinate system is fixed on the axis of the cylinder. The  $x$ -axis is directed downstream, the  $y$ -axis is perpendicular (defined as transverse) to the flow direction and the cylinder axis, and the  $z$ -axis lies along the axis of the cylinder (defined as spanwise).

Wake velocity measurements were made using a miniature hot-wire probe in conjunction with a two-channel anemometer system. The probe was mounted on a three-axis traversing mechanism which allowed it to be placed at any point in the wake. Oblique shedding angles were measured using two hot wires that were positioned at a known spanwise distance apart and offset in the streamwise direction such that each hot wire would experience the same phase of a passing oblique vortex, as indicated by Lissajous figures. A Stanford Research Systems SR760 spectrum analyser was used for the spectral measurements. Long-time-averaged velocity spectra were produced by averaging measured spectra for time durations in excess of 20 000 vortex shedding cycles. Fluctuating RMS velocities at the vortex shedding frequency were calculated using amplitudes of the corresponding spectral peak determined from long-time-averaged velocity spectra; it should be mentioned that the intensities at the higher harmonics of the shedding frequency were not included, since their intensity was typically less than 8% of the intensity of the fundamental frequency. The intensity of fluctuation at the shedding frequency,  $(u'_{rms}/U_\infty)_{f_k}$ , remains an excellent measure of the energy contained in the shedding mode. The total fluctuation intensity was measured on a Hewlett–Packard 3400A true-RMS meter with a frequency range of 10 Hz to 10 MHz. Time traces were recorded on a computerized data-acquisition system with a sampling rate of 10 kHz.

Flow visualization was conducted using a vertical smoke-wire system, as originally described by Corke *et al.* (1977). A GenRad 1540 Strobolume provided the intense illumination required to capture photographic images on ISO 400/27° film with a Nikon F3 camera.

### 3. The control of oblique and parallel vortex shedding

In order to demonstrate the control of shedding at Reynolds numbers beyond the laminar shedding regime, we begin with smoke-wire flow visualization at  $Re = 2000$ . By suitably manipulating the spanwise end conditions (endplates in the present study), it is possible to induce oblique shedding as shown in figure 1(*a*) and parallel shedding, shown in figure 1(*b*), over long spanlengths. Although clearly this is a simple result, it is nevertheless surprising that hitherto it was not known that one could control the spanwise shedding pattern at relatively high Reynolds numbers. The angle of shedding is controlled by the inclination of the right-hand endplate in figure 1(*a*). We find that by suitably angling this endplate, it is possible to induce mean shedding angles of up to 15°, as displayed in figure 2(*a*). We note here that even at these higher Reynolds numbers, the leading edges of the endplates need to be inclined inwards a finite amount before parallel shedding can be achieved, which is similar to the observation of Williamson (1989) in the laminar shedding regime. With an increase in shedding angle ( $\theta$ ), we find a decrease in the Strouhal number as shown in figure 2(*b*). This decrease of Strouhal number with increasing shedding angle, though not unexpected, has not been previously demonstrated for  $Re > 180$ . However, at these higher Reynolds numbers, there is some deviation from the cosine variation

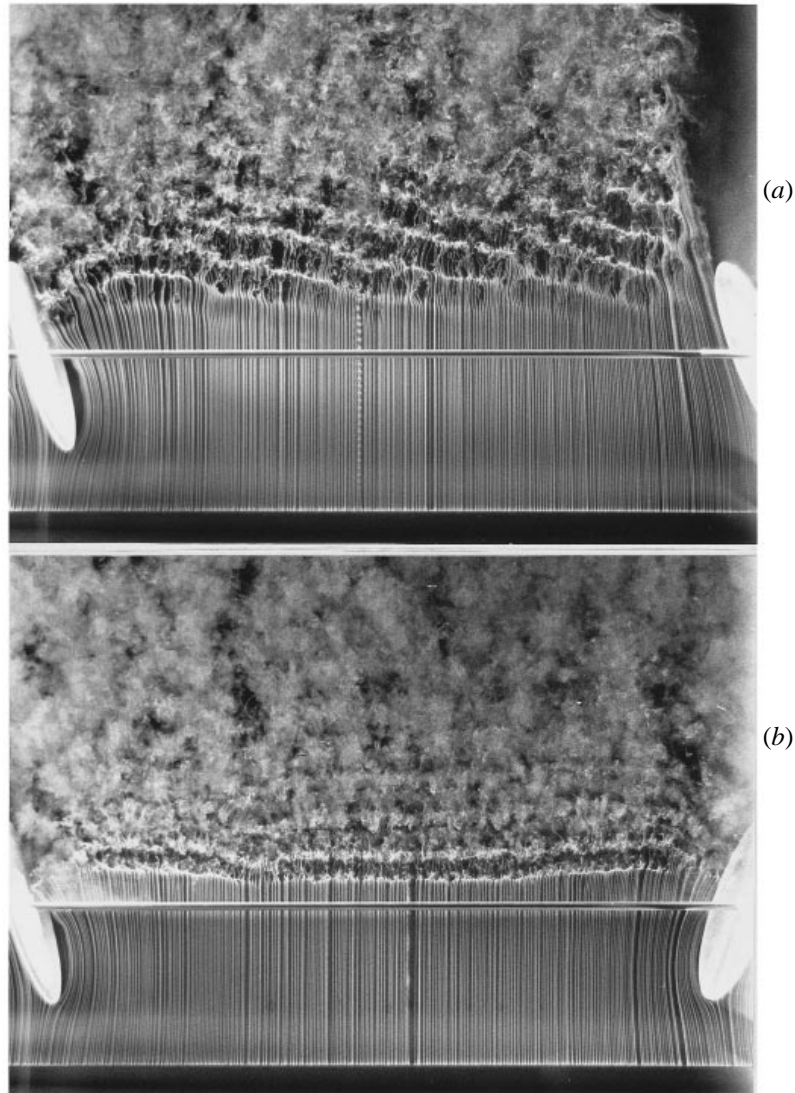


FIGURE 1. Smoke-wire flow visualization of the influence of the end conditions on the spanwise vortex shedding pattern at  $Re = 2000$ . (a) Oblique vortex shedding is induced across the entire span by inclining both endplates in the same direction. (b) Parallel shedding is induced by canting inwards the leading edges of both endplates. In both photographs, the flow is upwards and the smoke wire is positioned at  $x/D = -18$ ,  $y/D = 1.5$  ( $L/D = 80$ ).

(1), which is shown as the solid line in figure 2(b). In contrast to observations in the laminar shedding regime where the spectral bandwidth is unaffected, our measurements indicate that there is a remarkable difference in the development of velocity spectra with  $\theta$ , at higher  $Re$ . Spectra shown in figure 3 demonstrate that as the shedding angle is increased, the spectral bandwidth increases dramatically with a concomitant decrease in the peak value of the spectrum. (The spectral bandwidth ( $\Delta f_K$ ) is defined as the difference between the frequencies where the spectral level is 3 dB below the peak in the spectrum.)

One might question why there is a dramatic increase in spectral bandwidth as

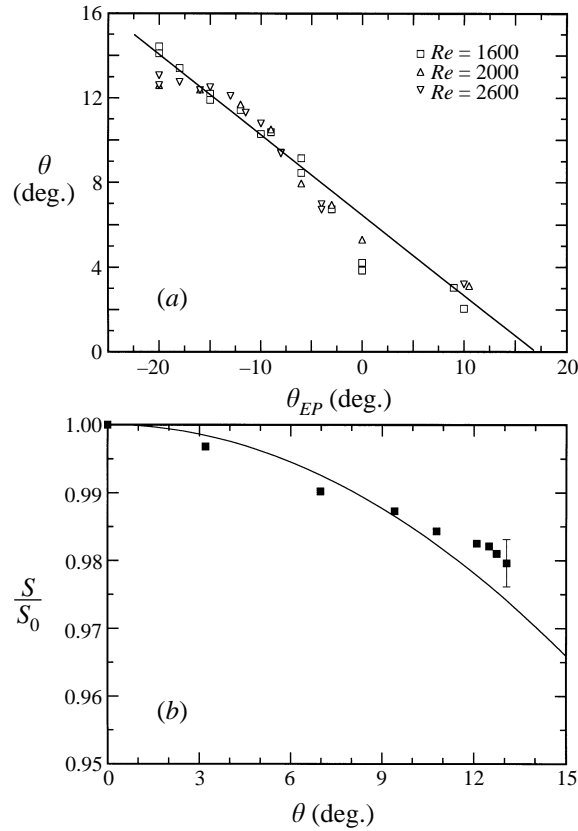


FIGURE 2. Characterization of the control of vortex shedding angle. (a) Variation of the shedding angle with angle of endplate. (b) Variation of Strouhal number with shedding angle at  $Re = 2600$ ;  $S_0$  is the Strouhal number for parallel shedding conditions. The solid line is the cosine transformation from (1), which accurately represents this variation in the laminar regime. At the largest value of shedding angle, the maximum estimated error in measuring Strouhal number has been displayed as an error bar. The measurements are made at  $x/D = 8$ ,  $y/D \approx 1.0$  ( $L/D = 80$ ).

oblique shedding angle increases. Flow visualization (not shown for this particular  $Re$ ) shows that the oblique vortex shedding angle is not constant, as it is in the laminar shedding regime, but varies slightly in time about a mean value. Furthermore, interspersed between instances of varying shedding angle, we find the appearance of sparse vortex dislocations along the span. It appears that the broadening of the spectrum with increasing shedding angle is due to a slight wavering of the shedding angle about a mean, and to the appearance of sparse dislocations induced by the end conditions. The increase in bandwidth and diminution of the spectral peak have been quantified respectively by a suitably normalized spectral bandwidth,  $\Delta f_K D^2/\nu$ , and by the intensity of fluctuation at the peak (shedding) frequency,  $(u'_{rms}/U_\infty)_{f_K}$ . We find that  $\Delta f_K D^2/\nu$  increases rapidly with shedding angle,  $\theta$ , as shown in figure 4(a), with a corresponding decrease in  $(u'_{rms}/U_\infty)_{f_K}$ , shown in figure 4(b). The results in figure 4 suggest that the spectral intensity, when integrated over all frequencies, may remain constant as shedding angle increases; as a matter of fact, we find that as  $\theta$  is increased, the total fluctuation intensity  $(u'_{rms}/U_\infty)_{Total}$  (which is a measure of the integrated spectral intensity) does remain very nearly constant, based on which

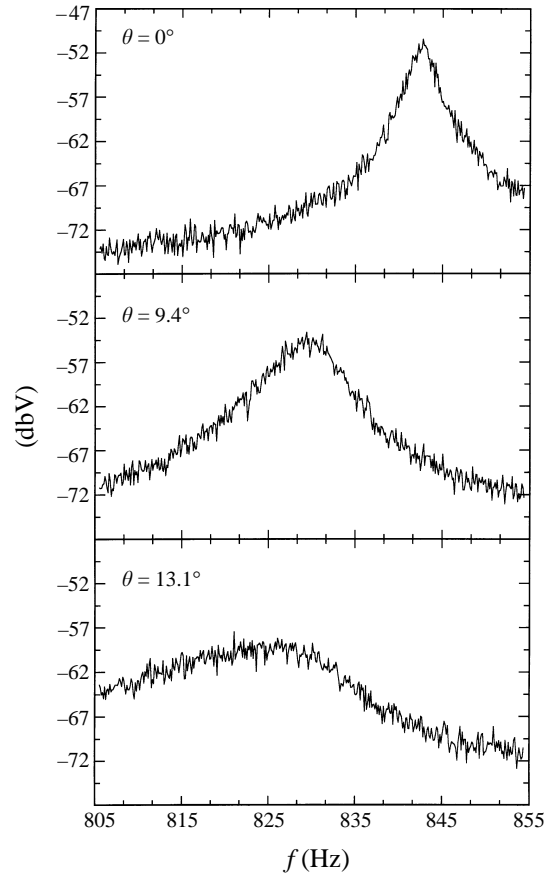


FIGURE 3. Development of the spectral peak at the shedding frequency with shedding angle at  $Re = 2600$ . All three spectra are identical in scale and the shedding angle corresponding to each spectrum is indicated. With increasing shedding angle, the spectral peak is observed to broaden dramatically, while its peak value diminishes simultaneously. The hot wire is positioned at  $x/D = 10$ ,  $y/D \approx 1.0$ .

one can conclude that at this particular  $Re$ , an increase in shedding angle causes a broader bandwidth of spectral energy around the shedding frequency.

Having demonstrated that wake measurements are indeed sensitive to the shedding angle, we now concentrate on a comparison of wake characteristic parameters obtained with conditions which produce the two extreme shedding angles. The label 'parallel shedding conditions' will hereafter refer to those which produce a zero shedding angle, whereas the label 'oblique shedding conditions' will be used to refer to those which induce a mean vortex shedding angle of about  $13^\circ$ – $15^\circ$ . It is clear that the oblique shedding end conditions would indeed induce some spanwise flow near the endplates.

In figure 5(a), we show contours of total fluctuation intensity in the near wake for the parallel shedding conditions at  $Re = 2600$ . Although not shown, contours of  $(u'_{rms}/U_\infty)_{Total}$  for oblique shedding conditions appear similar to those shown in figure 5(a), implying that the total turbulence intensity in the wake is not significantly altered by the end conditions, at this particular  $Re$ . However, the differences in turbulence intensity at the peak frequency, observed between parallel and oblique

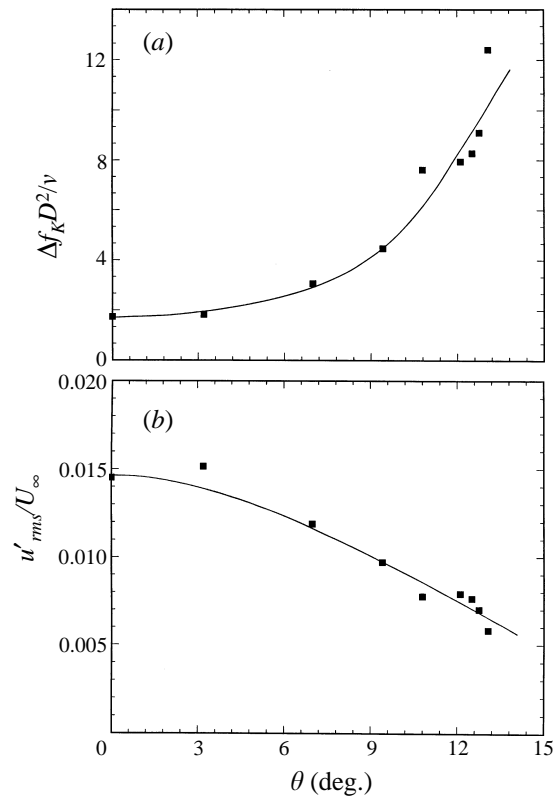


FIGURE 4. Characterization of the spectral peak at the shedding frequency. Variation of (a) normalized spectral bandwidth and (b)  $(u'_{rms}/U_\infty)_{f_K}$  with the vortex shedding angle, at  $Re = 2600$ . The hot-wire measurements are made at  $x/D = 10$ ,  $y/D \approx 1.0$ .

shedding end conditions (figure 4), which originate immediately behind the body, are found to persist for streamwise distances of around 40 diameters, as shown in figure 5(b). Transverse profiles of  $(u'_{rms}/U_\infty)_{f_K}$  were measured at various streamwise locations ( $x/D$ ); the maximum value of  $(u'_{rms}/U_\infty)_{f_K}$  across these profiles was selected and these data are presented in figure 5(b). Clearly, the parallel shedding conditions render a more coherent wake when compared to the oblique shedding conditions.

We have demonstrated above that it is possible to control the vortex shedding pattern at moderate Reynolds numbers. However, since many of our conclusions up to this point are based on measurements made at  $Re = 2600$ , we investigate the effect of end condition control over a wide range of  $Re$ , which is addressed in the following section.

#### 4. Wake velocity measurements over a large range of $Re$

The effect of the end conditions on the shedding pattern is characterized by a measurement of various wake parameters. We find that the Strouhal number is somewhat larger for parallel shedding conditions than it is for oblique shedding conditions, over almost the entire range of the Reynolds number displayed in figure 6. This indicates that there is indeed a control on the flow pattern over a whole range of  $Re$ . However, it is observed in figure 6 that the wake with parallel shedding

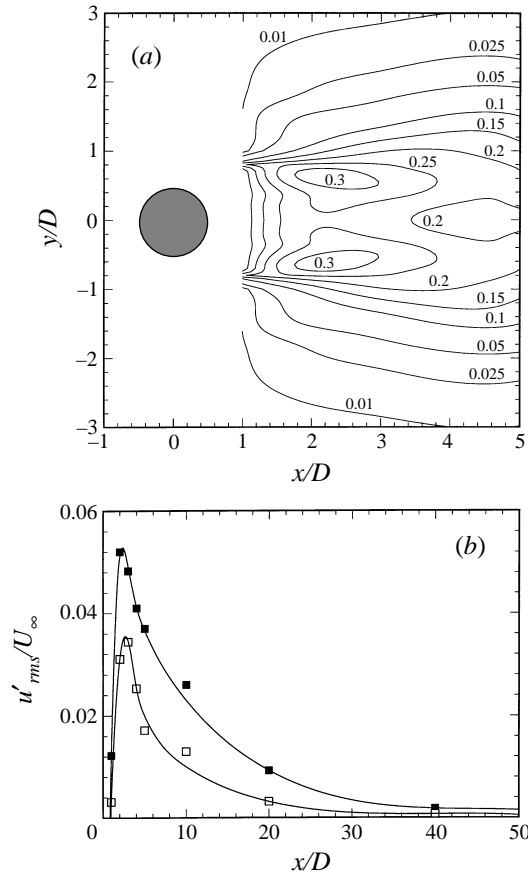


FIGURE 5. Downstream evolution of velocity fluctuations in the near wake at  $Re = 2600$ . (a) Contours of  $(u'_{rms}/U_{\infty})_{Total}$  for parallel shedding conditions. Similar results are obtained for oblique shedding conditions. (b) Variation of  $(u'_{rms}/U_{\infty})_{f_K}$ . At each streamwise location, transverse profiles of  $(u'_{rms}/U_{\infty})_{f_K}$  were measured. The data shown in (b) are the maximum value of  $(u'_{rms}/U_{\infty})_{f_K}$  across each transverse profile, with the solid symbols representing parallel shedding conditions and the open symbols representing oblique shedding conditions.

experiences a change of mode at  $Re \approx 5000$ , as demonstrated by the discontinuous decrease in the Strouhal number. This apparent change of mode is investigated in detail later (see §7). Although the measured values of  $S$  for oblique and parallel shedding are roughly similar beyond this transition, one cannot conclude that end manipulation does not affect the wake pattern for  $Re > 5000$ , as we discuss later.

In figure 7(a), we show the variation of  $(u'_{rms}/U_{\infty})_{Total}$  for a range of  $Re$ , from which it appears that the intensity for parallel shedding is slightly larger than for oblique shedding over most of the  $Re$ -range displayed. Our conclusions, in §3, regarding the constancy of  $(u'_{rms}/U_{\infty})_{Total}$  between parallel and oblique shedding, do not hold as one varies  $Re$  over a large range. However, the variation of  $(u'_{rms}/U_{\infty})_{f_K}$  shown in figure 7(b), indicates that the intensity for oblique shedding conditions is much smaller than that for parallel shedding conditions, over the entire  $Re$ -range. The local minimum in intensity observed at  $Re \approx 1200$  for parallel shedding conditions is associated with the inception of instability in the separated shear layers, and forms the subject of another investigation (Prasad & Williamson 1996). The transition at

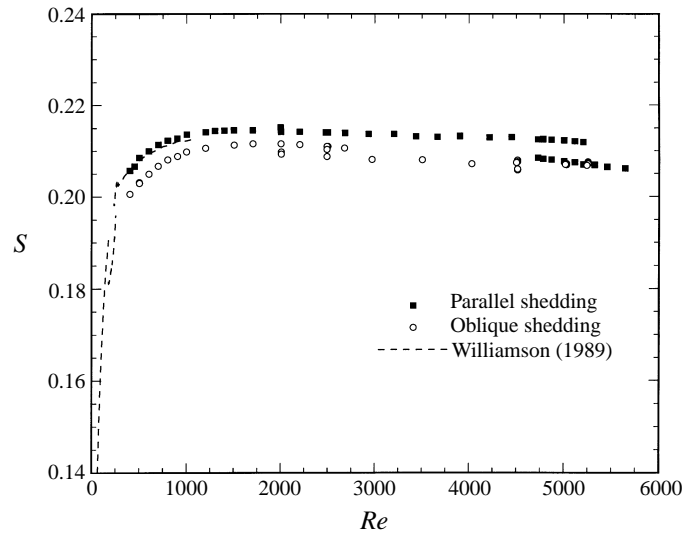


FIGURE 6. Strouhal number as a function of Reynolds number. Data for parallel and oblique shedding end conditions are shown over a large range of  $Re$ . A discontinuous decrease occurs for the parallel shedding case at  $Re = 5000$ . Data for  $Re < 450$  have been omitted for clarity, but shown by a broken line. The measurements are made at  $x/D = 10$ ,  $y/D = 1.0$ .

$Re \approx 5000$ , demonstrated by the discontinuity in the Strouhal number, seems to be associated with the gradual transfer of energy from one mode of shedding to another, as evidenced by the intersecting curves in figure 7(b), and will be discussed further in §7. However, even through this transition, the intensity for oblique shedding remains below that for parallel shedding.

The above discussion indicates that wake measurements display substantial differences between oblique and parallel shedding conditions, over a large range of Reynolds numbers. Data near the left-hand end of figures 6 and 7 have been intentionally omitted, since parameters vary rather rapidly in this range of  $Re$ . However, in the following sections, we focus on the rapid variation of parameters at these lower Reynolds numbers, beginning with the three-dimensional wake transition regime.

### 5. The wake transition regime

The wake transition regime ( $190 < Re < 260$ ) which is bounded by discontinuities in the Strouhal number, involves the inception of three-dimensionality in the form of small-scale mode-A and mode-B streamwise structures and large-scale vortex dislocations. The work of Williamson (1992, 1996b) has shown that vortex dislocations are spontaneously generated in the wake transition regime. We confirm their existence in the flow visualization at  $Re = 230$ , displayed in figure 8. These observations extend to all Reynolds numbers in the range  $190 < Re < 240$ , which suggests that there exists no spanwise end control on the vortex shedding pattern by the endplates in the wake transition regime, due to the presence of these dislocations.

However, one regains control on the shedding pattern near the upper end of the wake transition regime as we now explain. At  $Re = 260$ , the parallel shedding conditions induce a particularly spanwise-coherent mode of shedding, as shown in figure 9(a). Furthermore, time traces such as shown in figure 9(b) indicate that the shedding is virtually periodic. Both of these features are reminiscent of vortex

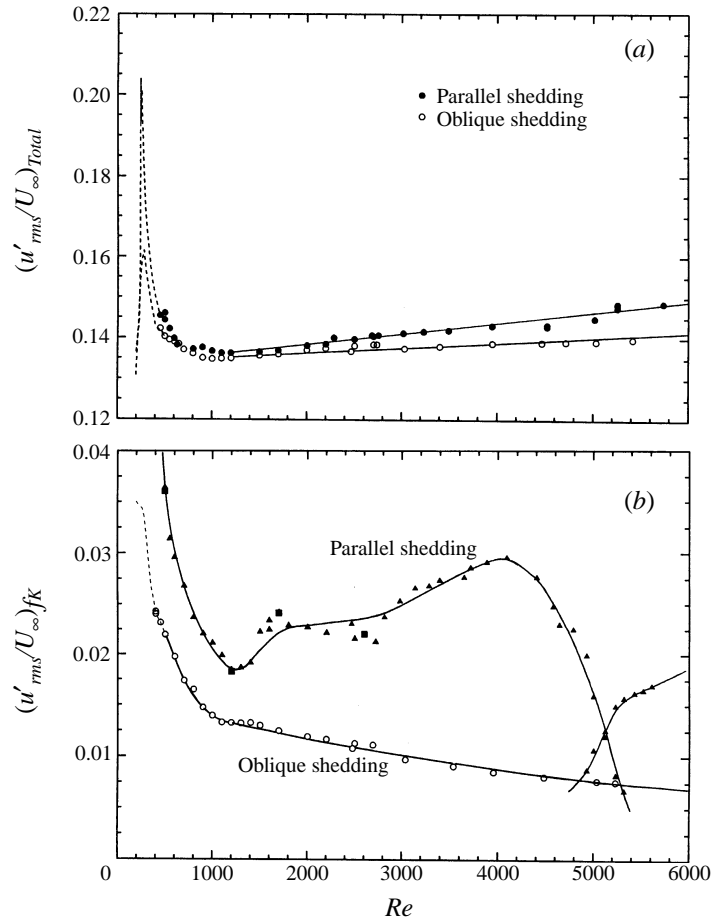


FIGURE 7. Variation of wake velocity fluctuation with  $Re$ . In (a) the intensity  $(u'_{rms}/U_\infty)_{Total}$  for parallel shedding conditions is comparable to that measured for oblique shedding conditions, over much of the Reynolds number range. However, in (b), the intensity  $(u'_{rms}/U_\infty)_{fK}$  is consistently larger for parallel shedding than for oblique shedding end conditions. For the case of parallel shedding, the local minimum at  $Re = 1200$  is associated with the inception of instability in the shear layers separating from the cylinder. The intersecting curves at  $Re \approx 5000$  are indicative of a gradual transfer of energy from one mode of shedding to another. In both cases, data for  $Re < 450$  have been intentionally omitted. The measurements are made at  $x/D = 10$ ,  $y/D = 1.0$ .

shedding observed in the laminar regime ( $49 < Re < 190$ ). Williamson (1996b) has shown that several wake parameters, including the base 'suction' coefficient (negative of base pressure coefficient) and the total fluctuation intensity, reach local maxima at  $Re = 260$ . In addition, he observed from flow visualization that the spanwise three-dimensional mode-B streamwise vortices are especially ordered at this  $Re$ . The particularly coherent mode of shedding obtained with parallel shedding conditions at  $Re = 260$ , produces the sharply peaked spectrum shown in figure 10(a).

On the other hand, with oblique shedding conditions imposed, the spectrum which is much broader and shown in figure 10(a), resembles spectra measured well within the wake transition regime for mode-A shedding. Furthermore, time traces measured at  $Re = 260$  for oblique shedding (not shown) display 'glitches', which are typical of the occurrence of dislocations observed within the wake transition regime for

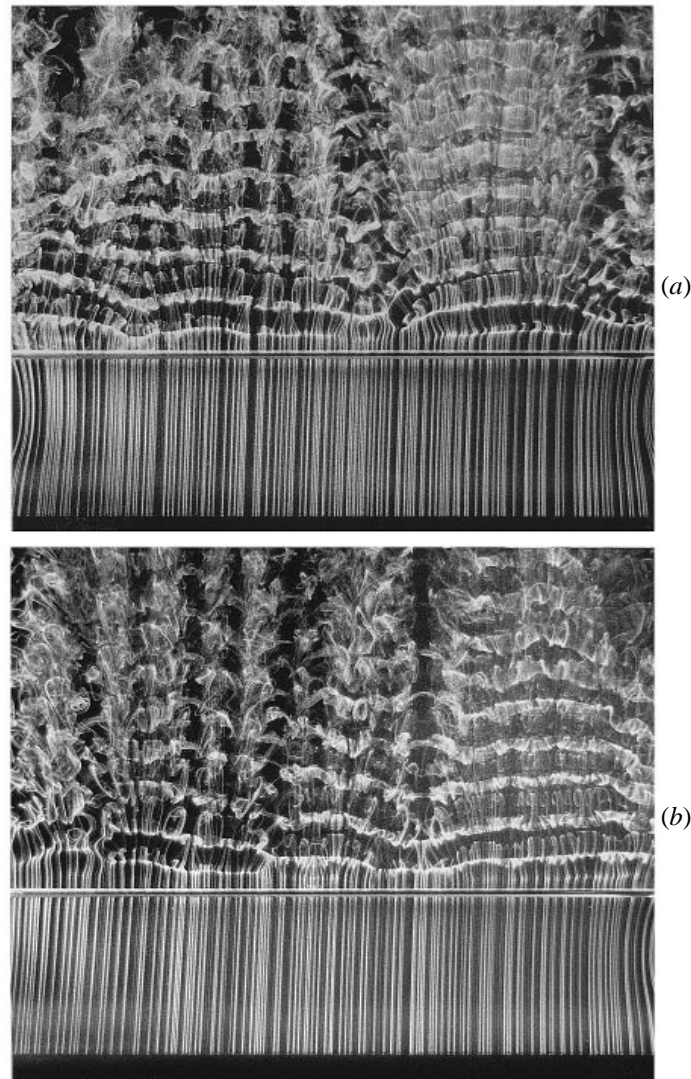


FIGURE 8. Demonstration that the presence of vortex dislocations precludes the possibility of end control of the shedding pattern in the wake transition regime, at  $Re = 230$ : (a) parallel shedding and (b) oblique shedding end conditions. In both photographs, the smoke wire is set at  $x/D = -18$ ,  $y/D = 0.5$  and  $L/D = 80$ .

mode-A shedding and the flow visualization clearly demonstrates the existence of vortex dislocations (figure 10*b*). Nevertheless, despite the formation of these vortex dislocations, there appears to be some control on the shedding angle, as is evident in figure 10*b*). In the absence of recognizing that dislocations are occurring for the oblique shedding boundary condition at  $Re = 260$ , one might be tempted to construe the lower frequency associated with figure 11 (relative to the parallel shedding case) as being due to oblique shedding effects only. However, at  $Re = 260$ , we measure  $S = 0.2053$  for parallel shedding conditions and  $S = 0.1937$  for oblique shedding conditions, which delivers an estimated shedding angle, using the transformation (1), of about  $20^\circ$ . On the other hand, our flow visualizations actually display typical

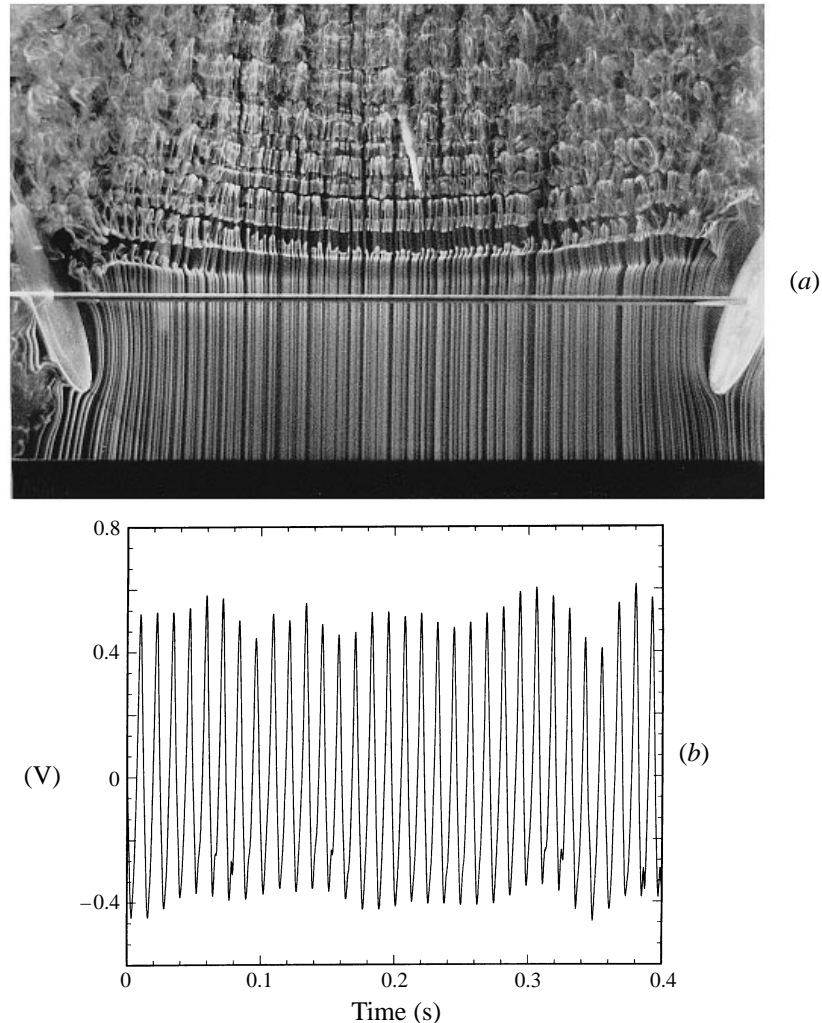


FIGURE 9. Flow features at  $Re \approx 260$  for parallel shedding conditions are reminiscent of those observed at lower  $Re$  in the laminar-shedding regime. In (a), flow visualization demonstrates the existence of a particularly spanwise-coherent vortex shedding pattern. The smoke wire is positioned at  $x/D = -18$ ,  $y/D \approx 0.5$ . The corresponding time trace in (b) indicates that velocity fluctuations are virtually periodic, producing the distinctly sharp peak in figure 10(a). The measurements are made at  $x/D = 8$  and  $y/D \approx 1.0$ . ( $L/D = 80$ ).

shedding angles of around  $8^\circ$ – $9^\circ$  (as shown in figure 10b near the oblique shedding end condition). Therefore, one can be clear from these results that it is the existence of dislocations in the flow which causes the large drop in frequency in figure 11. Indeed, dislocations can be identified from all our visualizations under these boundary conditions.

The regain of control on the shedding pattern for  $Re \geq 260$  is supported by the measurement of Strouhal number, presented in figure 11. The conditions of parallel shedding produce a discontinuity in  $S$  at the upper end of the transition regime, which is consistent with the measurements of Williamson (1988b, 1992), shown as the solid line. On the other hand, the oblique shedding conditions produce data which lie along

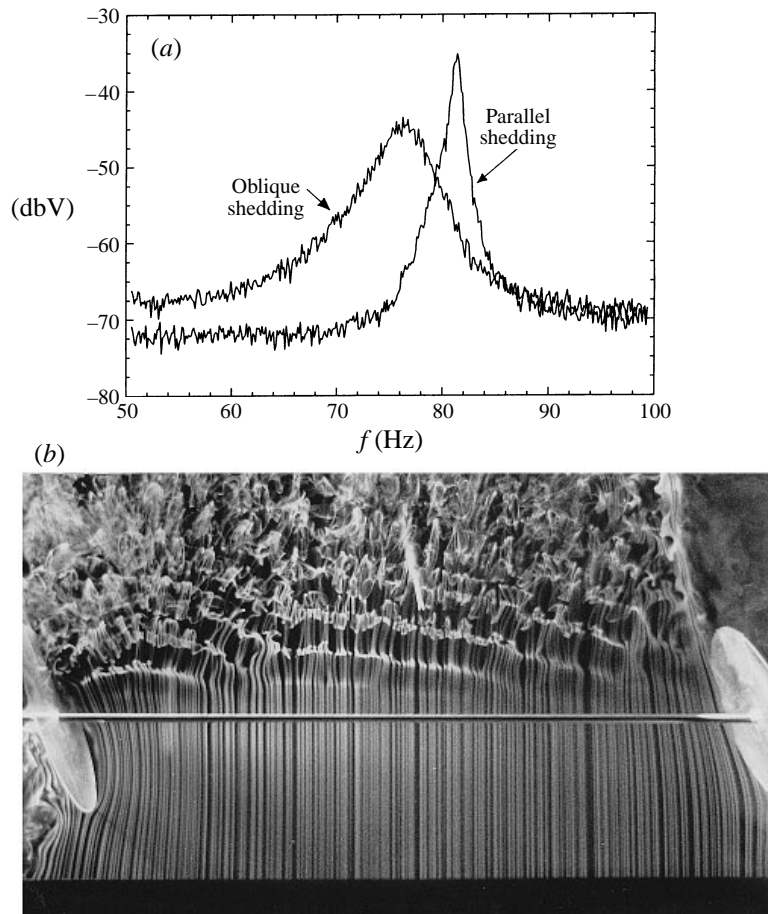


FIGURE 10. Flow features at  $Re \approx 260$  for oblique shedding conditions. In (a), the broad spectrum for oblique shedding arises due to the presence of dislocations which are induced by the end conditions. The measurements are made at  $x/D = 8.0$ ,  $y/D \approx 1.0$ . Flow visualization in (b) demonstrates that despite the presence of these dislocations, there appears to be some control on the shedding angle.  $x/D = -18$ ,  $y/D \approx 0.5$  and  $L/D = 80$ .

a line which is a smooth continuation of the mode-A Strouhal curve. This smooth extension suggests that the oblique shedding conditions promote the development of dislocations for  $Re > 260$ , where they would normally not occur. This has a practical significance, if one can deliberately decorrelate the vortex shedding through the inception of dislocations, and hence reduce the spanwise-integrated fluid forces on the body. It is surprising to note that the data of Leweke & Provansal (1995) for a torus coincide almost precisely with our oblique shedding data. There is the possibility that the requirement of periodic ends (physically realized in the case of a torus) cannot be easily met without the inception of dislocations, which causes the observed lower curve of Strouhal number. This is consistent with the low correlation (spanwise) for the torus wake at  $Re = 260$ .

Further evidence for the striking difference between parallel and oblique shedding conditions at the upper end of the wake transition regime is provided by a measurement of the intensity of velocity fluctuation. In figure 12(a), we display the variation of  $(u'_{rms}/U_\infty)_{Total}$  over a range of Reynolds numbers encompassing the laminar shedding

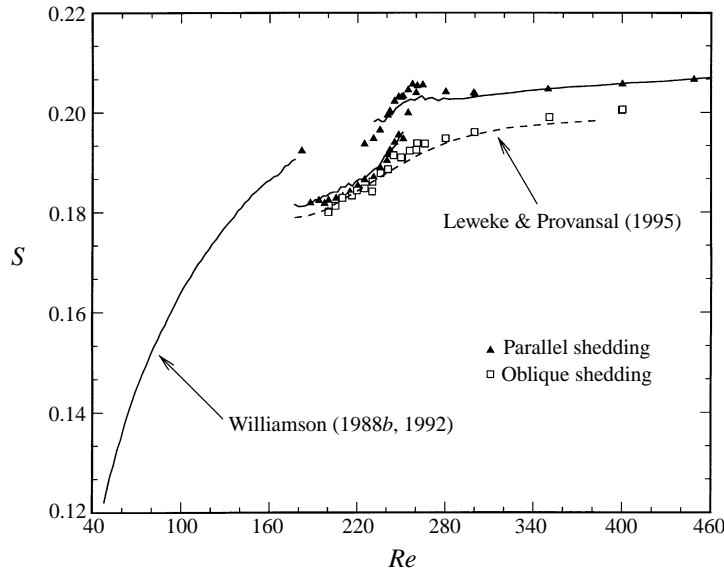


FIGURE 11. Variation of Strouhal number at low Reynolds numbers. The data from the present study confirm the presence of a discontinuity (Williamson 1988*b*) at  $Re = 230$ – $250$ , for parallel shedding conditions. On the other hand, data for oblique shedding appear to be a smooth extension of the Strouhal curve for mode A, and indicate that dislocations can be artificially induced by the end conditions, for  $Re > 260$ , where they would normally not occur. The measurements are made at  $x/D = 10.0$ ,  $y/D \approx 1.0$  with  $L/D = 80$ .

regime and the wake transition regime. We note from figure 12(*a*) that the variation of  $(u'_{rms}/U_\infty)_{Total}$  displays a remarkable maximum at  $Re \approx 260$  for parallel shedding and a subsequent decay with an increase in Reynolds number. It is interesting to note that this decay can be represented very nearly as  $(Re - 255)^{-0.1}$ ; although such a power law remains unexplained, it is indicative of the rate at which turbulence develops in the wake as  $Re$  increases. In much of the wake transition regime, the total fluctuation intensity measured with parallel shedding is nearly identical to that measured with oblique shedding, since dislocations are spontaneously generated along the span throughout this regime, irrespective of the end conditions. However, in the wake transition regime and for  $Re$  up to around 550, displayed in figure 12(*a*), the measurements for oblique shedding lie below those for parallel shedding. The variation obtained for parallel shedding conditions is qualitatively in agreement with the similar measurements of Williamson (1996*b*), although the maximum at  $Re \approx 260$  in the present study is considerably more accentuated with the use of parallel shedding conditions, which promote a particularly spanwise-coherent shedding mode. Furthermore, the present data are in good agreement with the DNS data of Henderson (1994) at  $Re = 500$  and data extracted from the measurements of Mansy, Yang & Williams (1994) at  $Re = 600$ , which are included in figure 12(*a*). The intensity of fluctuation at the shedding frequency,  $(u'_{rms}/U_\infty)_{f_K}$ , is found to be much larger for parallel shedding than for oblique shedding over the entire range of  $Re$ , as shown in figure 12(*b*). The data for parallel shedding clearly demonstrate a transfer of energy from mode A to mode B, as indicated by the intersecting curves, which arise due to the occurrence of a ‘twin-peak’ phenomenon in velocity spectra, as has been explained by Williamson (1988*b*, 1996*b*). We shall show in § 7 that the transition at  $Re \approx 5000$ , which also displays a twin-peak behaviour, resembles an inverse of this mode A to

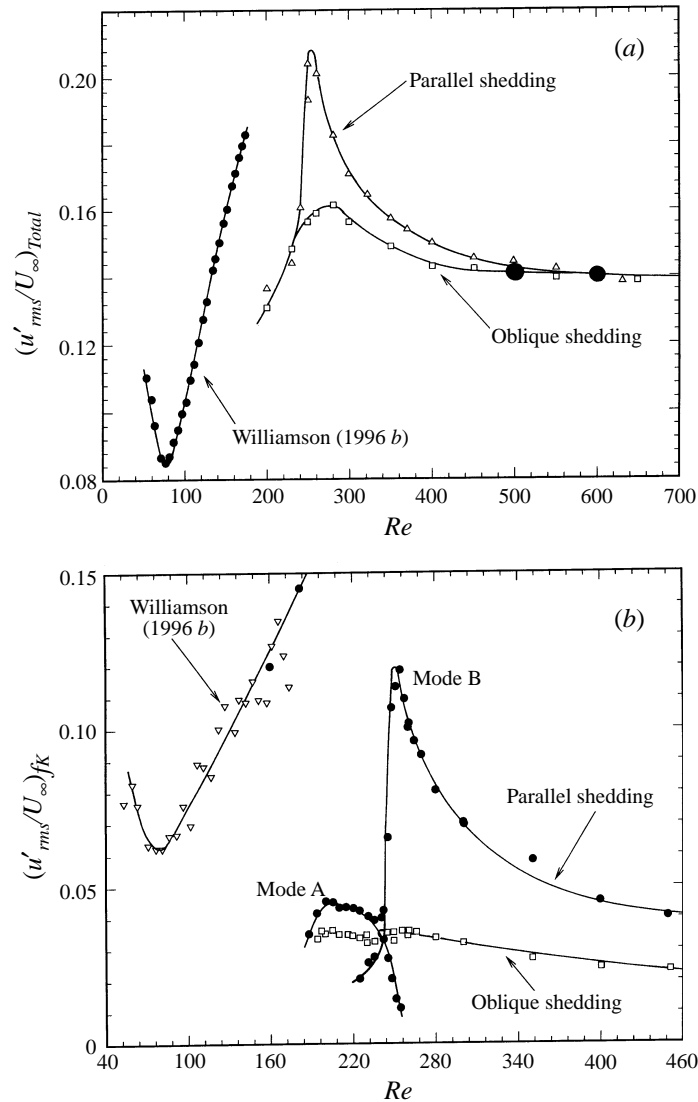


FIGURE 12. Variation of velocity fluctuation intensity with  $Re$ , at  $x/D = 10.0$  and  $y/D = 1.0$ . In (a), the intensity  $(u'_{rms}/U_\infty)_{Total}$  is nearly equal for the cases of oblique and parallel shedding conditions, over most of the wake transition regime. The remarkable peak at  $Re = 260$  is associated with the particularly coherent mode of shedding induced with parallel shedding conditions. The present data are found to compare well with the DNS data of Henderson (1994), shown as the solid symbol at  $Re = 500$ , and with the experimental data of Mansy *et al.* (1994), shown as the solid symbol at  $Re = 600$ . In (b), the intensity  $(u'_{rms}/U_\infty)_{f_K}$  is clearly higher for parallel shedding conditions than for oblique shedding conditions, over the entire range shown. Furthermore, the data for parallel shedding demonstrate the gradual transfer of energy from Mode A to Mode B, as evidenced by the intersecting curves near  $Re = 240$ , whereas for oblique shedding only a single curve is found.

mode B transition. However, in the wake transition regime, for the oblique shedding case, only a single curve is found, the level of which remains essentially unchanged over the range of  $Re$  shown in figure 12(b). It is necessary to point out here that the peak in  $(u'_{rms}/U_\infty)_{f_K}$  for parallel shedding conditions at  $Re = 260$  (in figure 12b), is comparable to values measured in the laminar shedding regime and is consistent

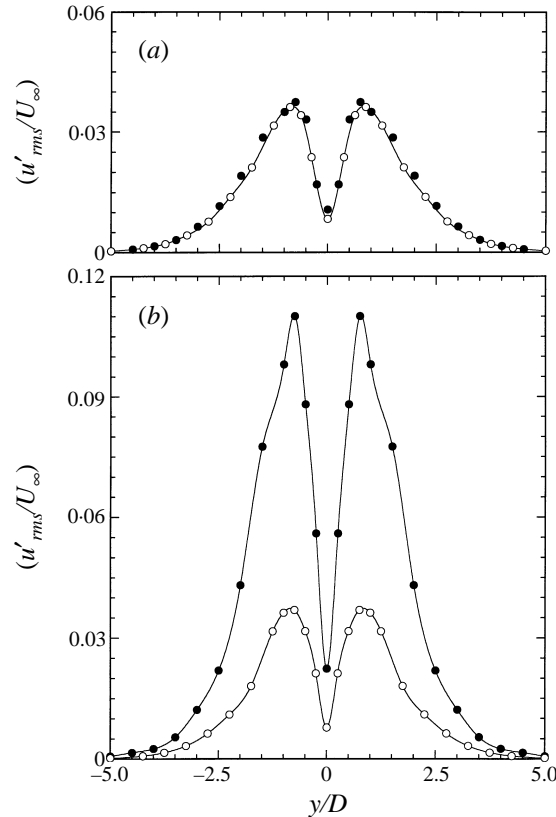


FIGURE 13. Influence of the end conditions on the transverse profile of  $(u'_{rms}/U_{\infty})_{f_K}$ , at  $x/D = 10$ , for (a)  $Re = 230$  and (b)  $Re = 260$ . Both plots are identical in scale. Symbols: parallel shedding (●) and oblique shedding (○).

with the observation from flow visualization that the vortex shedding is spanwise coherent.

One small point should be made regarding data presented in figure 12. It should be pointed out that the data taken from Williamson (1996b) measured in the laminar regime demonstrate the existence of a minimum at  $Re = 90$ . This is due to a rapid shrinking of the wake formation region at these low Reynolds numbers. It is the combination of the shrinking wake formation region and an increase in the intensity within this region that delivers a minimum at  $Re = 90$  in both figures 12(a) and 12(b), since the location of maximum turbulence intensity in the wake advances further upstream from the fixed position of measurement.

In order to show that the data presented in figure 12 are characteristic of the wake rather than the point of measurement, we present transverse velocity profiles in figure 13. The profiles measured at  $Re = 230$ , in figure 13(a), show that the intensity at all points across the wake is very similar for both oblique and parallel shedding conditions, and is consistent with a lack of control on the shedding pattern, at this  $Re$ . However, measurements at  $Re = 260$ , in figure 13(b), indicate that with parallel shedding, the wake is considerably more energetic across its entire width, as compared to oblique shedding. Furthermore, the profile measured with oblique shedding conditions at  $Re = 260$  resembles the profiles shown in figure 13(a), due to the inception of dislocations in each of these cases.

From the discussion above, one can conclude that over much of the wake transition regime, the presence of vortex dislocations precludes the control of wake shedding patterns through the use of spanwise end manipulation. The parallel shedding conditions promote a particularly spanwise coherent mode of shedding at  $Re = 260$ , whereas the oblique shedding conditions appear to extend the  $Re$ -range over which vortex dislocations are found.

## 6. The influence of aspect ratio

Our conclusions up to this point have been based on measurements made at midspan, in the wake of a cylinder with aspect ratios of 40–80. One naturally questions whether similar results would be obtained with larger aspect ratios. Before proceeding with our measurements for larger aspect ratio, we would like to begin with some observations made at a moderate  $Re = 500$  for  $L/D = 80$ . The two photographs in figure 14(a) are captured with the same experimental conditions, but at different instants in time. It appears that the vortex shedding angle is not constant but wavers slightly, which lends support to our earlier suggestion in §3. Interspersed between such occurrences of oblique shedding are found periods of dislocated shedding. However, time traces for oblique shedding, shown in figure 14(b), appear similar to those for parallel shedding (not shown), implying that at these Reynolds numbers, the somewhat chaotic appearance of the time traces, in both cases, precludes one from clearly distinguishing the presence or absence of vortex dislocations.

The influence of aspect ratio has been investigated in an indirect manner. The experiments were performed using a cylinder of aspect ratio fixed at  $L/D = 200$ . The hot-wire probe was traversed in the spanwise direction, with  $z$  being measured from the end condition which governs the oblique shedding angle. The case of parallel shedding conditions produced spectra which displayed no variation (of peak frequency or shape of peak) in the spanwise direction and the absence of dislocations. However, for oblique shedding conditions, measured spectra display variations in the spanwise direction, as shown in figure 15(a) for  $Re = 900$ , with similar results obtained for  $Re = 270$ . Figure 15(a) indicates that the spectrum at  $z/D = 35$  and  $Re = 900$  is very similar to the spectrum in figure 10(a) for oblique shedding conditions at  $Re = 260$ , whereas the spectrum at midspan ( $z/D = 100$ ) resembles that measured for parallel shedding conditions in figure 10(a). The spanwise variation of the peak in the velocity spectrum suggests a variation of the shedding angle along the span, as visualized in figure 15(b). The broadening of the spectrum as one moves from midspan towards the spanwise end which controls the shedding angle (the right-hand end in figure 15b), suggests that dislocations are induced by this end condition. We find that this end condition strongly influences larger portions of the span as one increases the endplate angle. This suggestion is based on our observation, from figure 15(b), that the number of dislocations per unit span is higher near  $z/D = 0$  than near midspan. In addition, from an examination of a series of spectra and time traces measured at various spanwise locations, including the ones presented in figure 15(a), it is observed that these dislocations occur more sparsely as distance from the end ( $z/D$ ) increases. To clarify this further, we now present the spanwise variation of Strouhal number at  $Re = 270$ , in figure 16(a). In this case, the Strouhal number measured using long-time-averaged velocity spectra is accurate to within about  $\pm 0.5\%$ . The endplate at  $z/D = 200$  is inclined at a fixed angle of  $+20^\circ$ . The inclination of the endplate at  $z/D = 0$  is varied between  $\theta_{EP} = -20^\circ$  (parallel shedding conditions) and  $\theta_{EP} = +20^\circ$  (oblique shedding conditions), with intermediate values of  $\theta_{EP}$  producing shedding

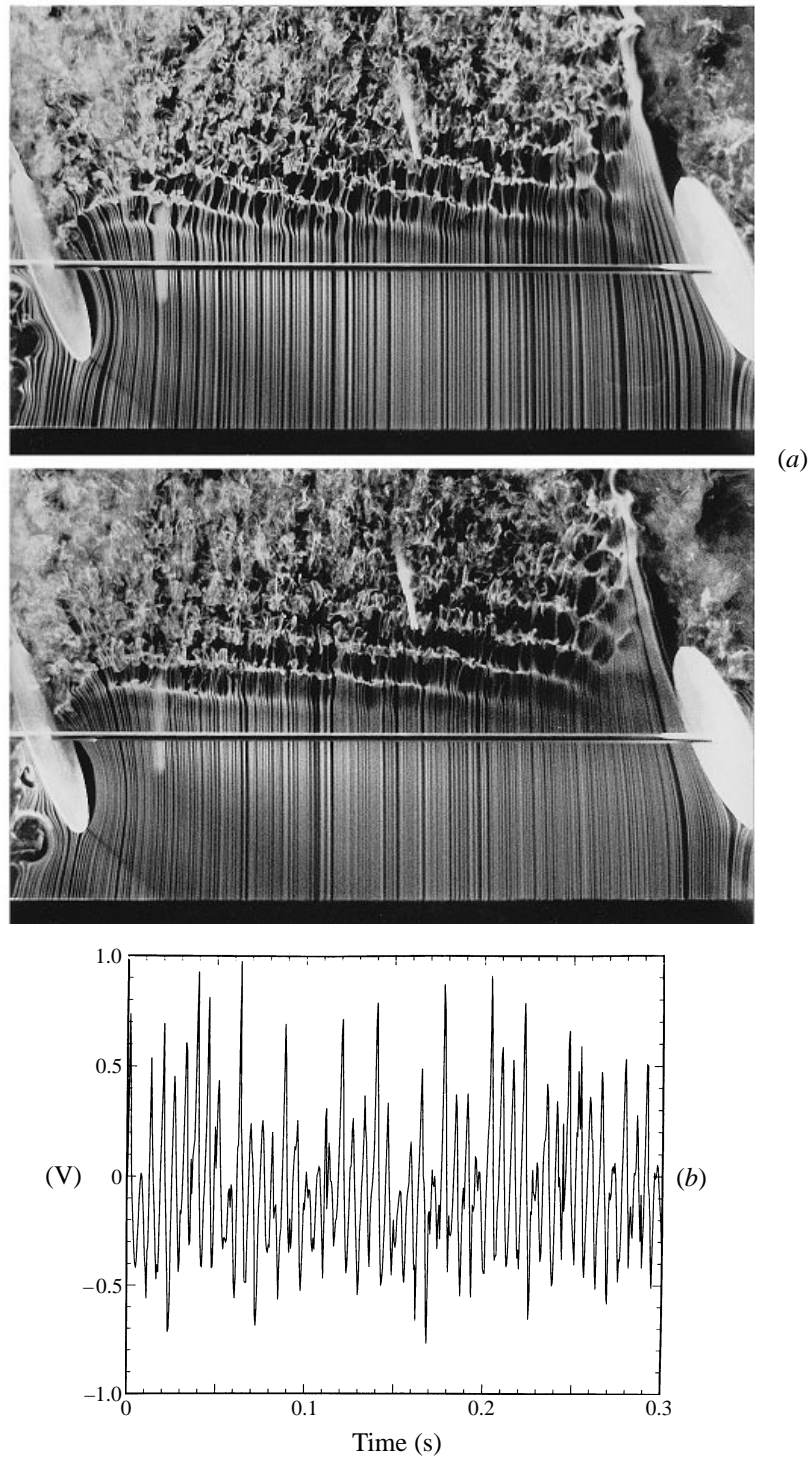


FIGURE 14. Control of oblique shedding at  $Re = 500$  for  $L/D = 80$ . The two images in (a) photographed with identical conditions but at different instants in time show that the oblique shedding angle wavers slightly. Interspersed between such events are found periods of dislocated shedding. The somewhat chaotic appearance of the time trace, in (b), obtained for oblique shedding conditions makes it difficult to distinguish the presence or absence of dislocations from time traces alone.

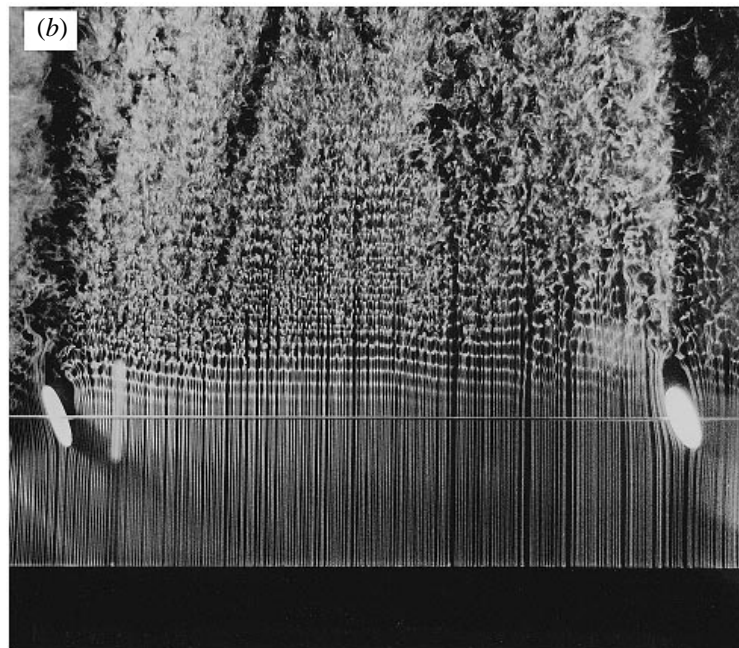
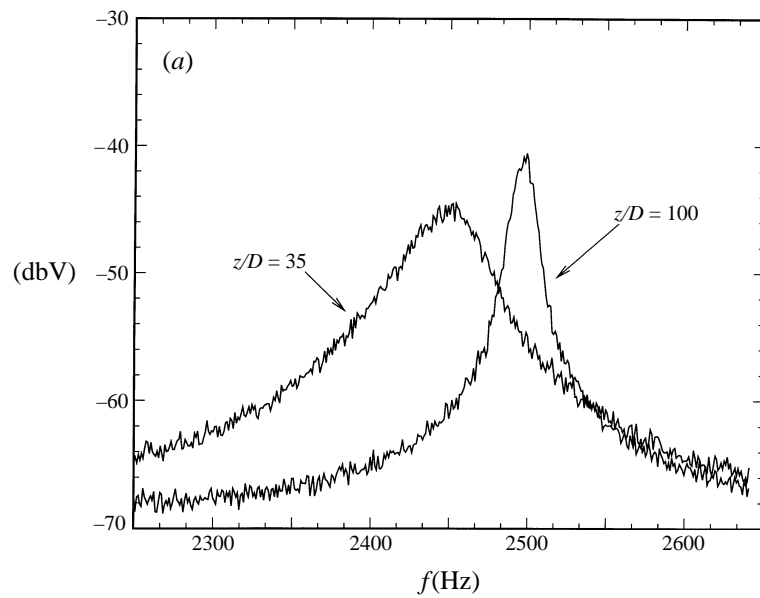


FIGURE 15. Flow features at  $L/D = 200$ . In (a), velocity spectra measured at  $x/D = 8$  for the oblique shedding conditions at  $Re = 900$  demonstrate that the spectral peak broadens as the right-hand end condition (at  $z/D = 0$ ) is approached. The right-hand end boundary condition, which governs the oblique shedding angle, also induces vortex dislocations. These dislocations are observed to be more numerous near this end condition than at midspan. Spanwise flow visualization at  $Re = 270$ , in (b), demonstrates that the oblique shedding angle varies across the span between the occurrence of dislocations. The smoke wire is placed at  $x/D = -48$ ,  $y/D \approx 1.0$  and the flow is upwards.

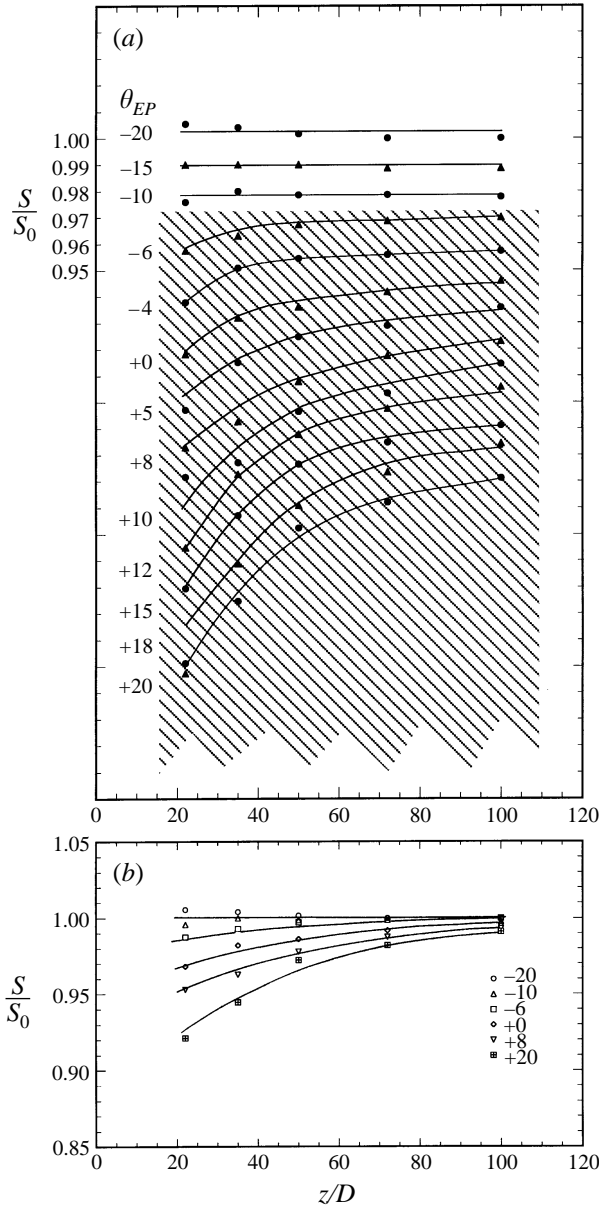


FIGURE 16. Spanwise variation of the Strouhal number at  $Re = 270$ . The normalized Strouhal number in (a), has been offset for each consecutive endplate angle by 0.01, to clarify the variation. The hatched area is that part of the span which is affected by the presence of dislocations. (b) The Strouhal number at midspan ( $z/D = 100$ ) is found to decrease as the endplate angle is increased, implying that the end conditions do induce a small oblique shedding angle in this region, despite the presence of dislocations. One end plate was maintained at a fixed angle while the angle of the other was varied from  $\theta_{EP} = -20$  to  $+20$ .  $L/D = 200$ .

angles between  $0^\circ$  and  $15^\circ$ . We find that as  $\theta_{EP}$  is increased beyond  $-6^\circ$ , the Strouhal number decreases smoothly from its midspan value as one approaches  $z/D = 0$ . The region which is affected by dislocations is indicated by the hatched area. Although the entire span appears to be affected by dislocations for  $\theta_{EP} > -6^\circ$ , the spanwise region near the end condition which governs oblique shedding ( $z/D = 0$ ) is affected more than the central portion of the span, as seen in figure 16(b). Dislocations occur in more abundance near the end condition at  $z/D = 0$  than at midspan. Figure 16(b) also indicates that the Strouhal number at midspan ( $z/D = 100$ ) decreases as the endplate angle increases from  $-20^\circ$  to  $+20^\circ$ , although the shape of the spectral peak at this location does not change. This implies that despite the occurrence of dislocations, the end condition induces a small oblique angle even at midspan, as can be seen in figure 15(b).

The above conclusions for the case of  $L/D = 200$  are consistent with our earlier results obtained at  $L/D = 40$ – $80$ . It appears that for all aspect ratios investigated, the parallel shedding conditions induce Kármán vortices which are spanwise parallel to the cylinder, with no evidence of dislocations in the range  $260 < Re < 5000$ . However, we find that the end condition which governs the oblique shedding angle induces dislocations that influence a large spanwise extent over the range of Reynolds numbers investigated; in the interval between the introduction of these dislocations, there exist periods of oblique shedding, for  $Re$  beyond the wake transition regime.

## 7. The transition at $Re = 5000$

Having addressed various aspects of wake characteristics over a wide range of Reynolds number, we now focus on the transition at  $Re \approx 5000$ , observed for the case of parallel shedding in figure 6, which is characterized by a discontinuous decrease in the Strouhal number. It needs to be reiterated that this transition is observed only for the case of parallel shedding conditions and not for oblique shedding conditions. Moreover, we show below that many wake parameters continue to be dissimilar between the two cases, even for  $Re > 5000$ . The intensity  $(u'_{rms}/U_\infty)_{f_K}$  in figure 7(b) displays intersecting curves for parallel shedding, which clearly indicates that a gradual transfer of energy occurs from one mode of shedding to another, through a 'twin-peak' phenomenon, which is explained presently. In contrast, the variation of  $(u'_{rms}/U_\infty)_{f_K}$  for oblique shedding conditions displays a single curve with an intensity much lower than for parallel shedding. Furthermore, it appears from figure 17 that the spectral bandwidth for oblique shedding is much larger than for parallel shedding, with the particular shape of the latter around  $Re \approx 5000$  being due to the phenomenon of twin-peak spectra. Therefore, despite our observation that the Strouhal number for parallel shedding conditions matches very closely the value for oblique shedding conditions, for  $Re > 5000$ , the wake structure appears to maintain differences between the two cases. However, in the discussion which follows, our attention will be directed only to the case of parallel shedding conditions. It will become apparent that our measurements confirm the existence of a transition originally suggested by Norberg (1987).

Norberg (1987, 1993) observed a rapid increase in the spectral bandwidth as  $Re$  increased beyond 5000, and proposed that the subcritical regime be demarcated into a 'lower'-subcritical regime ( $260 < Re < 5000$ ) and an 'upper'-subcritical regime ( $5000 < Re < 2 \times 10^5$ ). For reasons clarified in Norberg (1994), one can assume that the end conditions in his study promoted parallel shedding over the cylinder span. Norberg (1987) found that the Strouhal number decreases significantly above

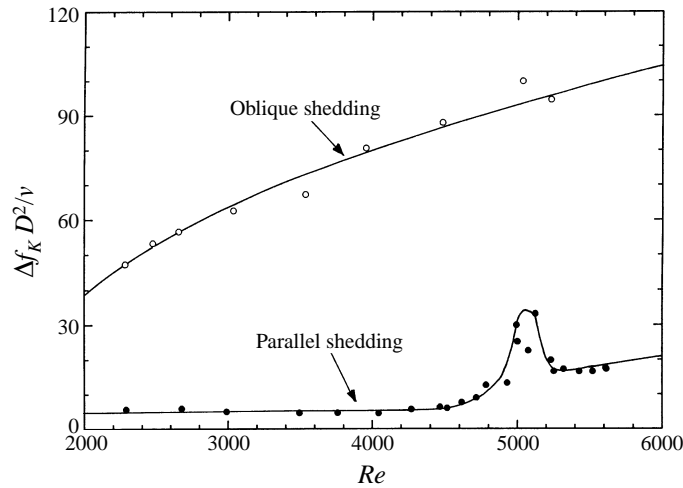


FIGURE 17. Variation of the normalized spectral bandwidth with  $Re$ . The spectral bandwidth for oblique shedding is considerably larger than for parallel shedding conditions. The shape of the curve near  $Re = 5000$ , for parallel shedding conditions, is associated with a change of shedding mode. The increased bandwidth for  $Re > 5000$  is due to the presence of dislocations. The measurements are made at  $x/D = 10$ ,  $y/D \approx 1.0$  and  $L/D = 40$ .

$Re = 5000$ , and continues to do so until the end of the subcritical regime. Although he did not observe the existence of a discontinuity in the Strouhal number, Norberg (1989) did suggest that the transition was probably related to a three-dimensional feature of the flow. To investigate this aspect, we have conducted spanwise flow visualization in the vicinity of this transition. We find that at  $Re = 4300$ , in figure 18(a), the end conditions do induce nearly spanwise coherent shedding across the span and especially in the region around midspan. However, at  $Re = 5300$ , vortex dislocations appear along the span, such as seen about one-third of the span from the left-hand end condition, in figure 18(b). Therefore, our flow visualizations indicate that the change of mode associated with the transition at  $Re = 5000$  is due to the development of vortex dislocations. In a related study, Norberg (1992) observed that dislocations develop in the region of a spanwise-discontinuous change in cylinder diameter for  $3000 < Re < 13\,000$ . Moreover, he showed from flow visualization that dislocations are present for  $Re > 5000$ , for the case of a *uniform* cylinder as well, which is in agreement with our observations. However, although the precise reason why dislocations manifest themselves for  $Re > 5000$  remains unexplained, one may suggest that the flow is susceptible to a three-dimensionality which is probably induced by the end conditions. In addition, one may question if these dislocations persist for all  $Re > 5000$ , or if indeed a further change of mode occurs at higher Reynolds numbers. Measurements from Norberg (1987) indicate that the axial correlation length decreases rapidly for  $Re > 5000$ , and till  $Re \approx 8 \times 10^4$ , which suggests that dislocations are found at least up to this  $Re$ . Szepessy (1994) has suggested that dislocations are present at  $Re \approx 4.3 \times 10^4$ , although it should be noted that his deductions were based on a smaller-aspect-ratio cylinder. However, further detailed measurements are necessary before one can conclusively state that dislocations are a fundamental feature of the cylinder wake flow in the 'upper'-subcritical regime.

In figure 19, we compare our measurement of  $S$  with those of Norberg (1987),

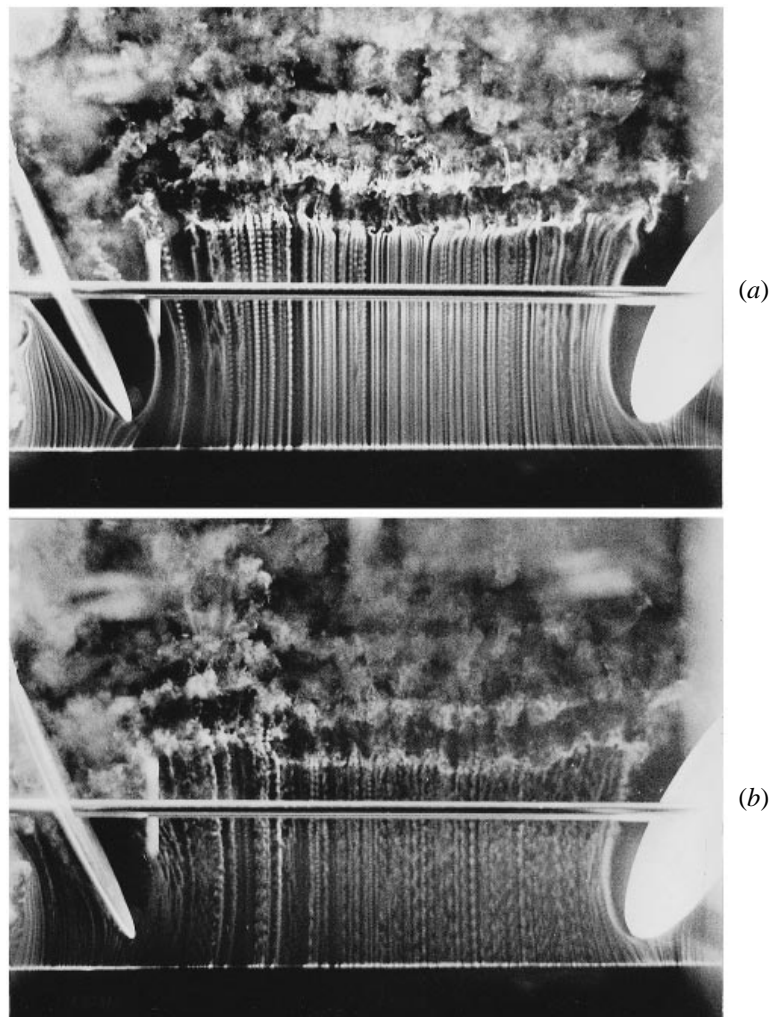


FIGURE 18. Visualization of flow features near  $Re = 5000$  for parallel shedding conditions. In (a), for  $Re = 4300$ , the shedding pattern appears spanwise coherent without dislocations. In (b), at  $Re = 5300$ , vortex dislocations appear along the span, seen at a location about  $1/3$  of the span from the left-hand endplate. The flow is upwards and  $L/D = 40$ .

measured for endplates oriented parallel to the streamwise direction. His data, which were measured for  $L/D = 120$ , do not display a discontinuity due the use of an algorithm which detected only a single spectral peak. Nevertheless, the resulting Strouhal number from his single-peak algorithm agrees well with our own measurements. A further observation we make from figure 19 is that the Strouhal number for the shedding mode in the range  $1000 < Re < 5000$  is virtually constant, whereas for the shedding mode at  $Re > 5000$ , it appears to decrease quite rapidly with Reynolds number, in agreement with the observations of Norberg (1987). Interestingly, Norberg (1994) found that Strouhal numbers measured at a series of aspect ratios all passed through a value of 0.21 at  $Re \approx 5000$ , and we observe from his measurements that the Strouhal number, for all values of aspect ratio, coincide for  $Re > 5000$  and at least up to  $Re = 30 \times 10^3$ . This suggests that the wake is insensitive to the proximity

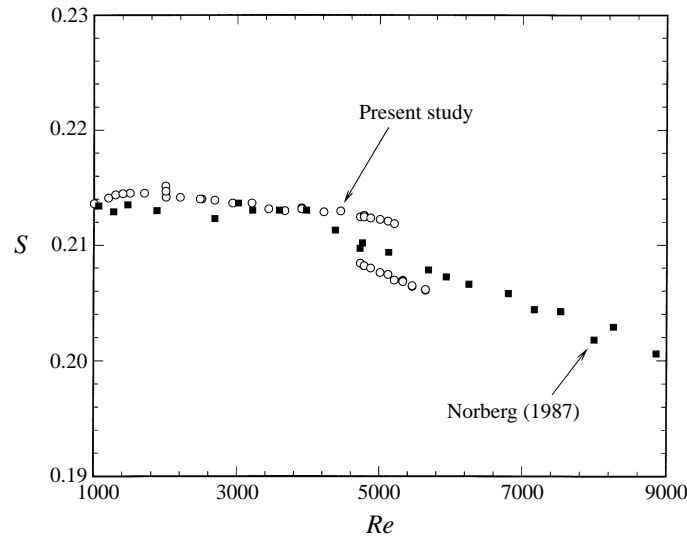


FIGURE 19. The discontinuous Strouhal curve near  $Re = 5000$ . The present data, measured at  $L/D = 40$ , for parallel shedding conditions are presented. The measurements of Norberg (1987) for  $L/D = 120$ , determined using a single-peak detection algorithm, are included.

of the end conditions, and lends support to the notion that dislocations may be a fundamental feature of the flow at these higher Reynolds numbers.

The ‘twin-peak’ phenomenon alluded to earlier refers to the simultaneous existence of two peaks in the spectrum, as shown in figure 20(a). The broken lines indicate the decay of one mode and the simultaneous growth of another, as  $Re$  is increased through 5000. It is the measure  $(u'_{rms}/U_\infty)_{peak}$  at each of these peaks that produces the intersecting curves in figure 7(b), which in turn display a remarkable similarity to the intersecting curves in the three-dimensional wake transition regime (figure 12b). The broken lines in figure 20(a) demonstrate the  $S-Re$  variation near the transition at  $Re = 5000$ , when the plot is viewed on its side. It is clear that the twin-peak phenomenon in figure 20(a) would produce the variation of spectral bandwidth shown in figure 20(b). We find that the measured bandwidth for  $Re > 5000$  is about twice as large as the value for  $Re < 5000$  which implies that the vortex shedding process becomes more incoherent as the Reynolds number is increased through 5000, and is consistent with the measurements of Norberg (1987). It is appropriate to mention here that although Norberg (1987) did not observe the twin-peak phenomenon at  $Re \approx 5000$ , it appears from other measurements (C. Norberg 1996, private communication) that such a behaviour may be quite sensitive to the free-stream turbulence level. At a very low turbulence level of 0.06%, C. Norberg (1996, private communication) has found evidence of a twin-peak behaviour in the range  $Re = 6000-8000$  that coincides with a plateau in the  $C_{P_B}-Re$  variation, which was demonstrated earlier by Norberg (1994). Several of the above observations indicate a distinct similarity between the transition at  $Re = 5000$ , and an *inverse* of the mode A to mode B transition found near the upper end of the three-dimensional wake transition regime, since each of these transitions involves

- a discontinuous decrease in Strouhal number;
- the observation of a phenomenon of twin-peak spectra;
- the inception of vortex dislocations.

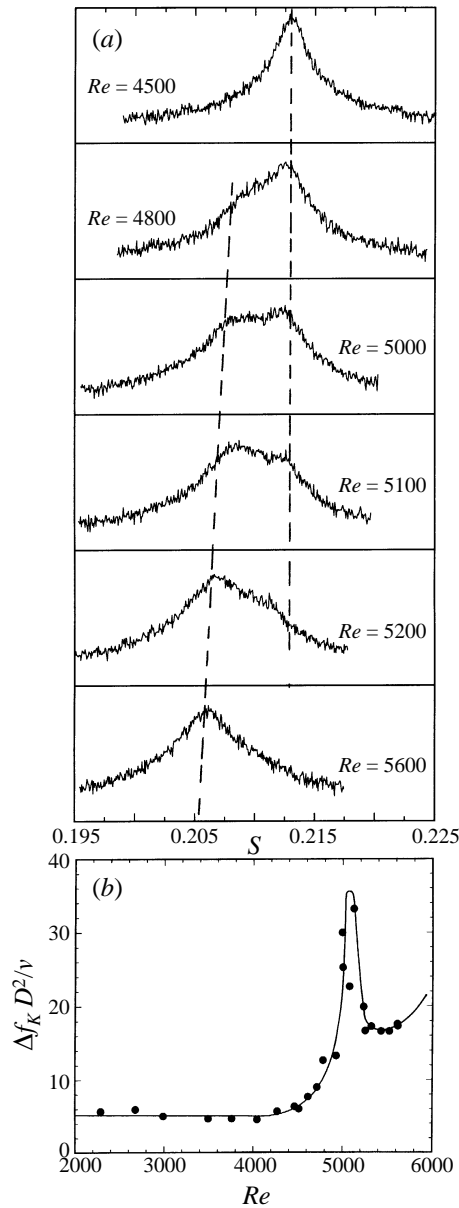


FIGURE 20. Spectral characteristics at  $Re$  across the transition at  $Re = 5000$ . Velocity spectra in (a) demonstrate clearly the gradual transfer of energy from one mode to another as  $Re$  is increased through 5000. This mode change is very similar to the inverse of the mode A to mode B transition. The ‘twin-peak’ behaviour is responsible for the shape of the spectral bandwidth curve that is presented in (b). The measurements are made at  $x/D = 10.0$ ,  $y/D = 1.0$  and  $L/D = 40$  for parallel shedding conditions.

Surprisingly, the change of shedding mode through the transition at  $Re = 5000$  influences the centreline velocities, as shown in figure 21. The centreline mean velocity, shown in figure 21(a), demonstrates the existence of a distinct plateau near  $x/D = 2$  for  $Re = 4473$ , but not for  $Re = 5427$ . The streamwise location of the plateau appears to coincide with the maximum in the centreline fluctuating velocity, shown in

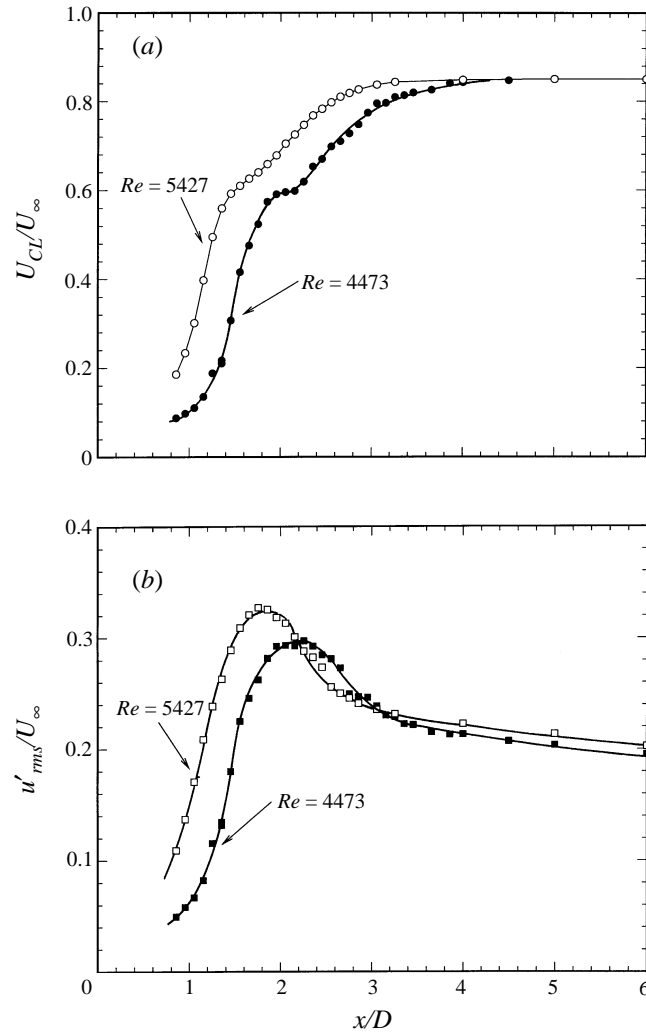


FIGURE 21. Streamwise evolution of normalized centreline velocity for Reynolds numbers near the transition at  $Re = 5000$ . In (a), the mean velocity,  $U_{CL}/U_{\infty}$ , displays a plateau for  $Re = 4473$ , but not for  $Re = 5427$ . The location of the maximum in  $(u'_{rms}/U_{\infty})_{Total}$  on the centreline in (b), which is one measure of the vortex formation length, almost coincides with the plateau in (a); it appears that vortex formation occurs closer to the cylinder for  $Re > 5000$  than for  $Re < 5000$ .  $L/D = 40$ .

figure 21(b). The streamwise distance to this maximum is one measure of the 'vortex formation length'. The data in figure 21(b) indicate that the vortex formation length decreases with increasing  $Re$ , in agreement with the measurements of Norberg (1987). Although, it is perhaps tempting to suggest that the non-existence of the plateau at  $Re > 5000$  is due to the inception of vortex dislocations, this may not be the case since we find from measurements made with parallel shedding conditions (but not shown) that the centreline mean velocity displays similar plateaus for both  $Re = 230$  and  $Re = 260$ .

In summary, it appears that the transition at  $Re \approx 5000$  is associated with the inception of dislocations which occur along the span, and in many respects resembles an inverse of the mode A to mode B transition found in the wake transition regime.

Although it is not clear exactly why these dislocations appear at  $Re = 5000$ , what can conclusively be stated is that the mode of shedding does undergo a fundamental change at this Reynolds number. One may question if our observation of this transition is perhaps linked to a coupling between the endplate wake and the wake of the cylinder, due to our use of only a moderate aspect ratio of  $L/D = 40$ , or if it is indeed a genuine feature of the flow. Strong support for the latter suggestion comes from the work of Norberg, wherein he clearly observed a transition at  $Re \approx 5000$  at aspect ratios of both 120 and 80; the endplates in his case were oriented parallel to the streamwise direction, which as one can imagine, produce a negligible interaction between the endplate wake and the cylinder wake.

## 8. Conclusions

In the present investigation, we have found that the primary vortex shedding from a cylinder can be controlled by manipulating the end conditions, for moderately high Reynolds numbers, in a manner not unlike that used in the laminar shedding regime ( $Re < 190$ ). Such control affects the frequency of the primary wake instability and its amplitude of fluctuation, as it does at low  $Re$ , although distinct differences are observed at the higher Reynolds numbers. We find that the imposition of oblique shedding end conditions at higher Reynolds numbers leads to a spatial variation of both the oblique angle and shedding frequency across the span and to dislocations which are not simply restricted to the spanwise end regions, as they are at low  $Re$ . These dislocations appear to become more sparsely occurring as one moves towards midspan, away from the end condition which governs the oblique shedding angle. The ability to promote the generation of dislocations, and to control the oblique angle of shedding has practical significance, if one can decorrelate the shedding along the span, to thereby deliver smaller spanwise-integrated unsteady fluid forces on the body. We find that inclining the leading edges of both plates inwards delivers parallel shedding over the entire span, that is free of dislocations in the range  $260 < Re < 5000$ .

In the wake transition regime, we confirm that in the range  $Re = 190$ – $250$ , the spontaneous appearance of dislocations in mode-A shedding precludes the control of shedding patterns using end manipulation. Furthermore, it has proven possible to extend the regime of Reynolds number where dislocations occur to  $Re > 250$ , by introducing them through end control, where they would otherwise not naturally occur. However, at  $Re = 260$ , the use of parallel shedding conditions induces a spanwise-uniform vortex shedding pattern which contains no dislocations, and a remarkable peak in the turbulence intensity measured in the wake, which is consistent with the suggestion of Williamson (1996*b*) that a ‘resonance’ may occur at this  $Re$ , when the primary wake frequency would be equal to the shear-layer frequency. We confirm the existence of a discontinuous variation in the Strouhal–Reynolds numbers relationship at the upper end of the wake transition regime found previously by Williamson (1988*b*), for the case of parallel shedding conditions. In contrast, we find that the imposition of oblique shedding conditions (which also induces dislocations) produces a smooth continuous Strouhal number curve as  $Re$  increases through 260. It appears that the discontinuous Strouhal variation around  $Re = 240$ – $260$  does indeed represent the infinite-aspect-ratio case, whereas the continuous variation for the torus wake of Leweke & Provansal (1995) coincides with our case when we induce vortex dislocations from the end conditions.

At higher Reynolds number, we confirm the existence of a transition in the mode of shedding at  $Re = 5000$ , originally found by Norberg (1987), under conditions of

parallel shedding. We show that this mode change, which demonstrates similarities with an *inverse* of the mode A to mode B transition found in the wake transition regime, involves the inception of vortex dislocations; however, it is not clear why the flow is unstable to such a mode. It appears that dislocations may be a feature of the flow, in the ‘upper’-subcritical regime (i.e.  $5000 < Re < 200\,000$ ) even under conditions of parallel shedding, although additional work is necessary to investigate this further.

The authors would like to express their deepest gratitude to Christoffer Norberg for several stimulating discussions regarding the transition at  $Re = 5000$ , and for making available to us some of his unpublished experimental data. We would also like to thank Thomas Leweke and Gregory Miller for valuable assistance during paper preparation. This work has been supported by the O.N.R. Grant Nos. N-00014-94-1-1197 and N-00014-95-1-0332.

## REFERENCES

- CORKE, T., KOGA, D., DRUBKA, R. & NAGIB, H. 1977 A new technique for introducing controlled sheets of streaklines in wind tunnels. *IEEE Publication 77-CH 1251-8 AES*.
- EISENLOHR, H. & ECKELMANN, H. 1989 Vortex splitting and its consequences in the vortex street wake of cylinders at low Reynolds number. *Phys. Fluids A* **1**, 189.
- GERICH, D. & ECKELMANN, H. 1982 Influence of end plates and free ends on the shedding frequency of circular cylinders. *J. Fluid Mech.* **122**, 109.
- HAMMACHE, M. & GHARIB, M. 1991 An experimental study of the parallel and oblique vortex shedding from circular cylinders. *J. Fluid Mech.* **232**, 567.
- HENDERSON, R. D. 1994 Unstructured spectral element methods: parallel algorithms and simulations. PhD thesis, Dept. of Mech. & Aero. Engng, Princeton University.
- KÖNIG, M., EISENLOHR, H. & ECKELMANN, H. 1990 The fine structure in the  $S$ - $Re$  relationship of the laminar wake of a circular cylinder. *Phys. Fluids A* **2**, 1607.
- LEWEKE, T. & PROVANSAL, M. 1995 The flow behind rings: bluff body wakes without end effects. *J. Fluid Mech.* **288**, 265.
- LEWEKE, T. & WILLIAMSON, C. H. K. 1996 Elliptic instability and three-dimensional transition in bluff body wakes. Submitted to *Phys. Rev. Lett.*
- MANSY, H., YANG, P.-M. & WILLIAMS, D. R. 1994 Quantitative measurements of spanwise-periodic three-dimensional structures in the wake of a circular cylinder. *J. Fluid Mech.* **270**, 277.
- MILLER, G. D. & WILLIAMSON, C. H. K. 1994 Control of three-dimensional phase dynamics in a cylinder wake. *Exps. Fluids* **18**, 26.
- MONKEWITZ, P. A., WILLIAMSON, C. H. K. & MILLER, G. D. 1996 Phase dynamics of Kármán vortices in cylinder wakes. *Phys. Fluids* **8**, 91.
- NORBERG, C. 1987 Effects of Reynolds number and a low-intensity free stream turbulence on the flow around a circular cylinder. Publ. 87/2. Dept. of Applied Thermodynamics and Fluid Mechanics, Chalmers University of Technology.
- NORBERG, C. 1989 An experimental study of the circular cylinder in cross flow: transition around  $Re = 5 \times 10^3$ . In *Proc. 4th Asian Congress of Fluid Mechanics, Suppl. Vol., C240, University of Hong Kong*.
- NORBERG, C. 1992 An experimental study of the flow around cylinders joined with a step in the diameter. In *Proc. 11th Australasian Fluid Mechanics Conf., University of Tasmania*.
- NORBERG, C. 1993 Pressure forces on a circular cylinder in cross flow. In *Proc. IUTAM Symp. Bluff-Body Wakes, Dynamics and Instabilities, Göttingen* (ed. H. Eckelman, J. M. R. Graham, P. Huerre & P. A. Monkewitz), p. 275. Springer.
- NORBERG, C. 1994 An experimental investigation of the flow around a circular cylinder: influence of aspect ratio. *J. Fluid Mech.* **258**, 287.
- PRASAD, A. & WILLIAMSON, C. H. K. 1996 The instability of the separated shear layer from a bluff body. *Phys. Fluids* **8**, 1347.

- PROVANSAL, M., MATHIS, C. & BOYER, L. 1987 Bénard–von Kármán instability: transient and forced regimes. *J. Fluid Mech.* **182**, 1.
- STÄGER, R. & ECKELMANN, H. 1991 The effect of endplates on the shedding frequency of circular cylinders in the irregular range. *Phys. Fluids A* **3**, 2116.
- SZEPESSY, S. 1994 On the spanwise correlation of vortex shedding from a circular cylinder at high subcritical Reynolds number. *Phys. Fluids* **6**, 2406.
- WILLIAMSON, C. H. K. 1988*a* Defining a universal and continuous Strouhal–Reynolds relationship for the laminar vortex shedding of a circular cylinder. *Phys. Fluids* **31**, 2742.
- WILLIAMSON, C. H. K. 1988*b* The existence of two stages in the transition to three-dimensionality of a cylinder wake. *Phys. Fluids* **31**, 3165.
- WILLIAMSON, C. H. K. 1989 Oblique and parallel modes of vortex shedding in the wake of a circular cylinder at low Reynolds numbers. *J. Fluid Mech.* **206**, 579.
- WILLIAMSON, C. H. K. 1992 The natural and forced formation of spot-like ‘vortex dislocations’ in the transition of a wake. *J. Fluid Mech.* **243**, 393.
- WILLIAMSON, C. H. K. 1996*a* Vortex dynamics in the cylinder wake. *Ann. Rev. Fluid Mech.* **28**, 477.
- WILLIAMSON, C. H. K. 1996*b* Three-dimensional wake transition. *J. Fluid Mech.* **328**, 345.